

Short Communication

Preparation and Corrosion Property of $\text{Co}_{68}\text{Fe}_{7-x}\text{Cr}_x\text{Si}_{15}\text{B}_{10}$ Amorphous Alloy

Xiaowei Liang¹, Xiang Li^{2,*}, Chen Chen², Zheng Liang², Chao Xiong³, Yuxin Wang^{1,*}

¹School of Materials Science and Engineering, Tongji University, Shanghai 200092, China

²School of Materials Science and Engineering, University of Shanghai for Science and Technology, Shanghai, China

³School of Photoelectric Engineering, Changzhou Institute of Technology, Changzhou 213002, China

*E-mail: xiangliusst@163.com, ywan943@aucklanduni.ac.nz

Received: 27 May 2015 / Accepted: 15 July 2015 / Published: 26 August 2015

$\text{Co}_{68}\text{Fe}_{7-x}\text{Cr}_x\text{Si}_{15}\text{B}_{10}$ ($x=0, 1.5, 3, 4.5$) amorphous ribbons were prepared by melt-spinning technique. Influences of Cr content on the soft magnetic property and corrosion resistance under sulfuric acid were systematically studied. Results indicate that after adding Cr elements, the coercivity of alloys was decreased significantly. The addition of Cr element can greatly improve the corrosion resistance of Co-Fe-Si-B amorphous alloys. $\text{Co}_{68}\text{Fe}_4\text{Cr}_3\text{Si}_{15}\text{B}_{10}$ has the best soft magnetic property and lowest hysteresis loss with significant improved corrosion resistance.

Keywords: Co-based amorphous alloy, Soft magnetic property, Corrosion resistance

1. INTRODUCTION

Co-based amorphous alloys with good soft magnetic properties have been widely used in many magnetic devices and electronic equipment, such as transformer magnetic devices, sensors and switching power supplies [1-5]. These magnetic devices and electronic equipment often work in a variety of acidic, alkaline or neutral corrosive environments, which increases the requirement of the corrosion resistance of the amorphous alloys. Much effort has been devoted to the improvement of their corrosion resistance without sacrificing magnetic properties, either by modification of the heat treatment conditions or by substitution of the different constituting elements in recent years [6-8]. The existing research results have proved that proper addition of Cr in the alloy can significantly increase the corrosion property of alloy as it can form a Co-rich passivation film.

In the present work, traditional Co-Fe-Si-B alloy was selected as the object of analysis. By adding different amounts of Cr instead of Fe, four different kinds of Co-Fe-Cr-Si-B amorphous alloys including $\text{Co}_{68}\text{Fe}_7\text{Si}_{15}\text{B}_{10}$, $\text{Co}_{68}\text{Fe}_{5.5}\text{Cr}_{1.5}\text{Si}_{15}\text{B}_{10}$, $\text{Co}_{68}\text{Fe}_4\text{Cr}_3\text{Si}_{15}\text{B}_{10}$ and $\text{Co}_{68}\text{Fe}_{2.5}\text{Cr}_{4.5}\text{Si}_{15}\text{B}_{10}$ were prepared. Their soft magnetic property and corrosion resistance in sulfuric acid were systemically studied.

2. EXPERIMENTAL DETAILS

2.1 Sample preparation

Master alloy ingots with four different compositions ($\text{Co}_{68}\text{Fe}_7\text{Si}_{15}\text{B}_{10}$, $\text{Co}_{68}\text{Fe}_{5.5}\text{Cr}_{1.5}\text{Si}_{15}\text{B}_{10}$, $\text{Co}_{68}\text{Fe}_4\text{Cr}_3\text{Si}_{15}\text{B}_{10}$ and $\text{Co}_{68}\text{Fe}_{2.5}\text{Cr}_{4.5}\text{Si}_{15}\text{B}_{10}$) were casted by vacuum arc melting furnace (ArcMelter, Germany). The as-obtained alloy ingots were cut into small pieces and polished before putting into vacuum melt-spun furnace. The ribbons with 10 mm wide and 20 μm thick were fabricated by using melt spinning technique on a single roller copper-wheel melt-spinning system (Sky, China) under Ar atmosphere. The schematic drawing of melt-spinning device was shown in Fig. 1. The related parameters of melt-spinning were listed in Table 1.

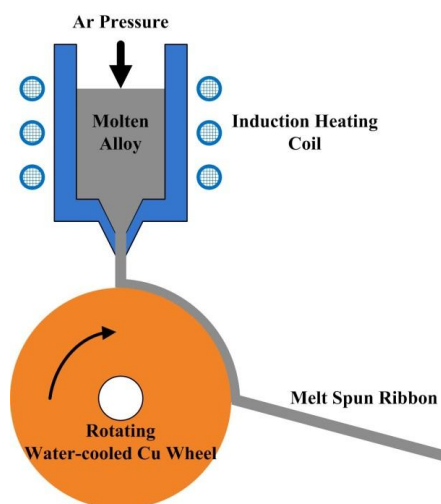


Figure 1. Schematic drawing of melt-spinning device

Table 1. Processing parameters for melt-spinning

Processing parameters	Quantity
Rotation speed	5000 rpm
Nozzle length	5 mm
Quartz tube length	162 mm
Vacuum degree	5.5×10^{-3} Pa
Current density	50 A
Injection pressure	0.06 MPa

2.2 Sample characterization

The surface morphologies and composition were analyzed using a field emission scanning electron microscope (FEI Quanta 200) with an energy-dispersive spectroscopy (EDS) system. The phase structure, average grain size and preferred orientation of coatings were determined by XRD using (D2 Bruker X-ray diffractometer) operated at 30 kV and 10 mA with the Cu-K α radiation. B-H analyzer was used to determine the soft magnetic properties of the ribbons. The electrochemical tests were conducted in an electrochemical workstation (Parstat2273) using a classical three-electrode system. Potentiodynamic polarization tests were carried out at a scan rate of 1 mVs⁻¹ at room temperature in a 5 wt. % H₂SO₄ solution. AC impedance test was obtained with frequency range of 100000–0.01 Hz. Magnetic properties were measured with DC B-H loop tracer (model BHS-40, Riken) with high sensitivity under a field of 800 A/m.

3. RESULTS AND DISCUSSION

3.1 Microstructure

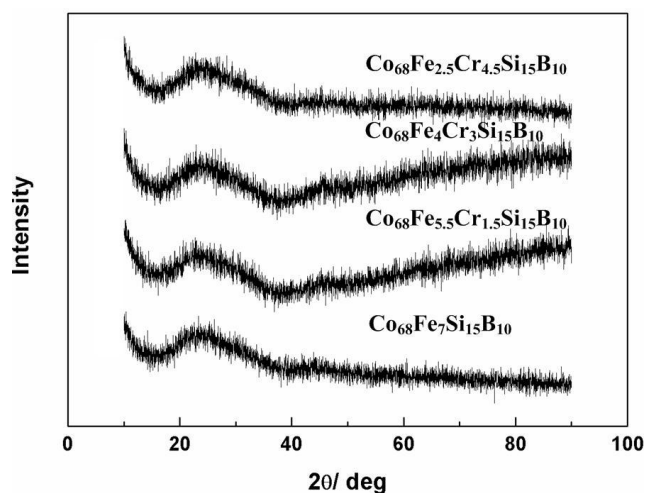


Figure 2. XRD spectrum of Co₆₈Fe_{7-x}Cr_xSi₁₅B₁₀ alloy

Fig. 2 shows the XRD patterns of Co₆₈Fe_{7-x}Cr_xSi₁₅B₁₀ alloys. All the Co₆₈Fe_{7-x}Cr_xSi₁₅B₁₀ ribbons present a clear amorphous structure and broaden diffraction peak. The addition of Cr doesn't cause a deterioration of metal glass forming ability. No crystallization peaks can be seen in the patterns which indicate a good metallic glass forming ability. The predominant amorphous plane of the alloys is located in 22° which is consistent with the other types of Co based amorphous alloy.

3.2 Soft magnetic properties

Table 2 presents the soft magnetic properties of Co₆₈Fe_{7-x}Cr_xSi₁₅B₁₀ alloys. In general, the smaller of the coercivity, the better soft magnetic property of the amorphous alloy. The coercivity of Co₆₈Fe₇Si₁₅B₁₀ is relatively high, ~7.19 A/m. After adding Cr elements, the coercivity of alloys was

decreased significantly. $\text{Co}_{68}\text{Fe}_4\text{Cr}_3\text{Si}_{15}\text{B}_{10}$ has the best soft magnetic property and lowest hysteresis loss as it has the lowest coercivity ($H_c=0.1305$ A/m) and the smallest remanence ($B_r=0.0163$ T).

Table 2. Soft magnetic properties of $\text{Co}_{68}\text{Fe}_{7-x}\text{Cr}_x\text{Si}_{15}\text{B}_{10}$ alloys

	$\text{Co}_{68}\text{Fe}_7\text{Si}_{15}\text{B}_{10}$	$\text{Co}_{68}\text{Fe}_{5.5}\text{Cr}_{1.5}\text{Si}_{15}\text{B}_{10}$	$\text{Co}_{68}\text{Fe}_4\text{Cr}_3\text{Si}_{15}\text{B}_{10}$	$\text{Co}_{68}\text{Fe}_{2.5}\text{Cr}_{4.5}\text{Si}_{15}\text{B}_{10}$
H_m (A/m)	795.8	795.8	795.8	795.7
B_m (T)	0.3554	0.4113	0.3611	0.2314
B_r (T)	0.1056	0.0923	0.0163	0.0331
H_c (A/m)	7.19	3.91	0.1305	3.18

3.3 Corrosion resistance

3.3.1 Open circuit potential curves

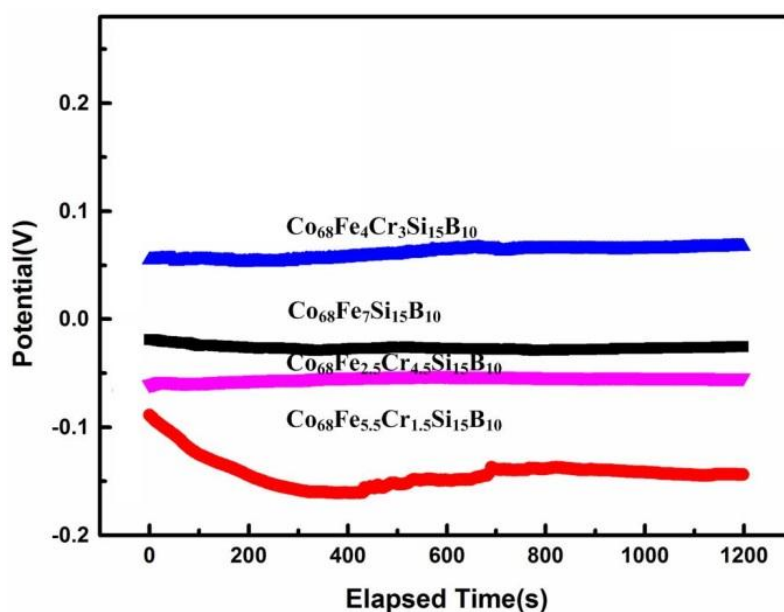


Figure 3. Open circuit potential of $\text{Co}_{68}\text{Fe}_{7-x}\text{Cr}_x\text{Si}_{15}\text{B}_{10}$ alloys in 5% H_2SO_4 solution

OCP is actually the equilibrium potential of the electrode when there is no net current flow in the circuit, a measure of the nobility of materials [9-11]. Fig. 3 shows the open circuit potential curve of $\text{Co}_{68}\text{Fe}_{7-x}\text{Cr}_x\text{Si}_{15}\text{B}_{10}$ alloy recorded in 5% H_2SO_4 solution. It can be seen that when the ribbon specimens were initially immersed into the H_2SO_4 solution, the electrochemical system was stable except $\text{Co}_{68}\text{Fe}_{5.5}\text{Cr}_{1.5}\text{Si}_{15}\text{B}_{10}$, evidenced by the negative shift of the OCP. After immersed into the H_2SO_4 solution more than 700 seconds, the OCP value of specimens became stable. $\text{Co}_{68}\text{Fe}_{5.5}\text{Cr}_{1.5}\text{Si}_{15}\text{B}_{10}$ possesses the most negative value (~ -0.15 V) of the OCP, while $\text{Co}_{68}\text{Fe}_4\text{Cr}_3\text{Si}_{15}\text{B}_{10}$ has the most positive value (~ 0.06 V).

3.3.2 Potentiodynamic polarization curves

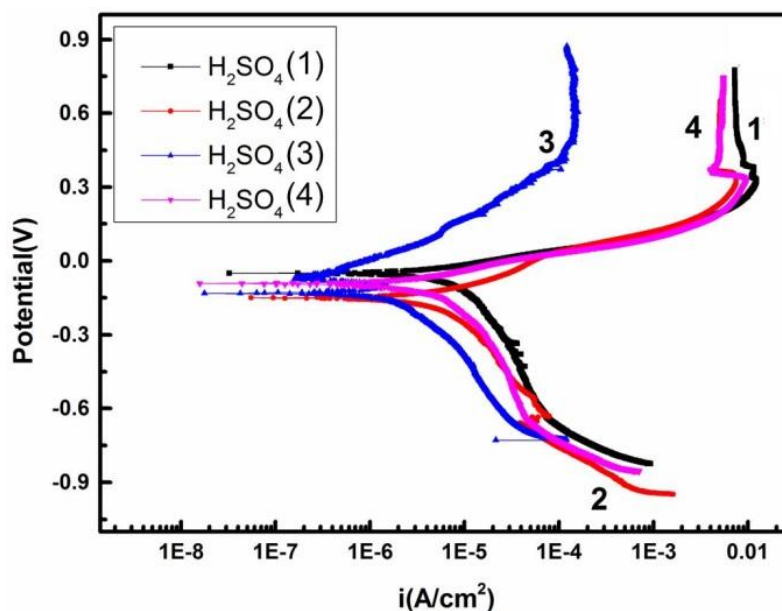


Figure 4. Potentiodynamic polarization curves of $\text{Co}_{68}\text{Fe}_{7-x}\text{Cr}_x\text{Si}_{15}\text{B}_{10}$ alloys in 5% H_2SO_4 solution: (1) $\text{Co}_{68}\text{Fe}_7\text{Si}_{15}\text{B}_{10}$, (2) $\text{Co}_{68}\text{Fe}_{5.5}\text{Cr}_{1.5}\text{Si}_{15}\text{B}_{10}$, (3) $\text{Co}_{68}\text{Fe}_4\text{Cr}_3\text{Si}_{15}\text{B}_{10}$ and (4) $\text{Co}_{68}\text{Fe}_{2.5}\text{Cr}_{4.5}\text{Si}_{15}\text{B}_{10}$.

The potentiodynamic polarization curves of $\text{Co}_{68}\text{Fe}_{7-x}\text{Cr}_x\text{Si}_{15}\text{B}_{10}$ alloys are shown in Fig. 4. Table 3 presents the electrochemical parameters. The polarization cathodic Tafel lines of $\text{Co}_{68}\text{Fe}_7\text{Si}_{15}\text{B}_{10}$, $\text{Co}_{68}\text{Fe}_{5.5}\text{Cr}_{1.5}\text{Si}_{15}\text{B}_{10}$, and $\text{Co}_{68}\text{Fe}_{2.5}\text{Cr}_{4.5}\text{Si}_{15}\text{B}_{10}$ gradually decrease to a lower polarization current density values with the increasing potential. When potential value is over self-corrosive potential, the corrosion current increases dramatically which indicate the corrosion rate increases remarkably. As for the cathodic part of Tafel line for $\text{Co}_{68}\text{Fe}_4\text{Cr}_3\text{Si}_{15}\text{B}_{10}$, the corrosion rate is general same as the others, however, the corrosion current kept a same level with the increasing potential. Additionally, there is no passivation process occurs during the test. The optimum addition of Cr element was considered to be 3 at.%, where the corrosion potential was -0.131 V and the corrosion current density was about $8.2 \times 10^{-7} \text{ A/cm}^2$.

Table 3. Electrochemical parameters of potentiodynamic polarization curves calculated from the Tafel extrapolation method.

Sample	E_{corr} (V vs. SCE)	I_{corr} ($\times 10^{-6} \text{ A/cm}^2$)
$\text{Co}_{68}\text{Fe}_7\text{Si}_{15}\text{B}_{10}$	-0.049	9.638
$\text{Co}_{68}\text{Fe}_{5.5}\text{Cr}_{1.5}\text{Si}_{15}\text{B}_{10}$	-0.149	6.194
$\text{Co}_{68}\text{Fe}_4\text{Cr}_3\text{Si}_{15}\text{B}_{10}$	-0.131	0.820
$\text{Co}_{68}\text{Fe}_{2.5}\text{Cr}_{4.5}\text{Si}_{15}\text{B}_{10}$	-0.077	3.120

3.3.3 Electrochemical impedance spectroscopy

Fig. 5 shows the electrochemical impedance spectrums (EIS) of $\text{Co}_{68}\text{Fe}_{7-x}\text{Cr}_x\text{Si}_{15}\text{B}_{10}$ alloys. The Nyquist plots of impedance expressed mainly as a single capacitive loop with different compounds and concentrations. The EIS results of $\text{Co}_{68}\text{Fe}_{7-x}\text{Cr}_x\text{Si}_{15}\text{B}_{10}$ alloys show a same tendency with the Tafel plots. As has been reported before [12-16], the larger radius of capacitive impedance loop, the higher polarization resistance, R_p and better corrosion resistance which characterizes the charge transfer across the electrolyte–electrode interface. It can be seen that $\text{Co}_{68}\text{Fe}_4\text{Cr}_3\text{Si}_{15}\text{B}_{10}$ has the best polarization resistance as it possesses the largest capacitive impedance loop. Correspondingly, $\text{Co}_{68}\text{Fe}_7\text{Si}_{15}\text{B}_{10}$ possesses the worst polarization resistance since its radius of capacitive impedance loop is the smallest. The addition of Cr causes a significant effect on the EIS of $\text{Co}_{68}\text{Fe}_{7-x}\text{Cr}_x\text{Si}_{15}\text{B}_{10}$ alloys.

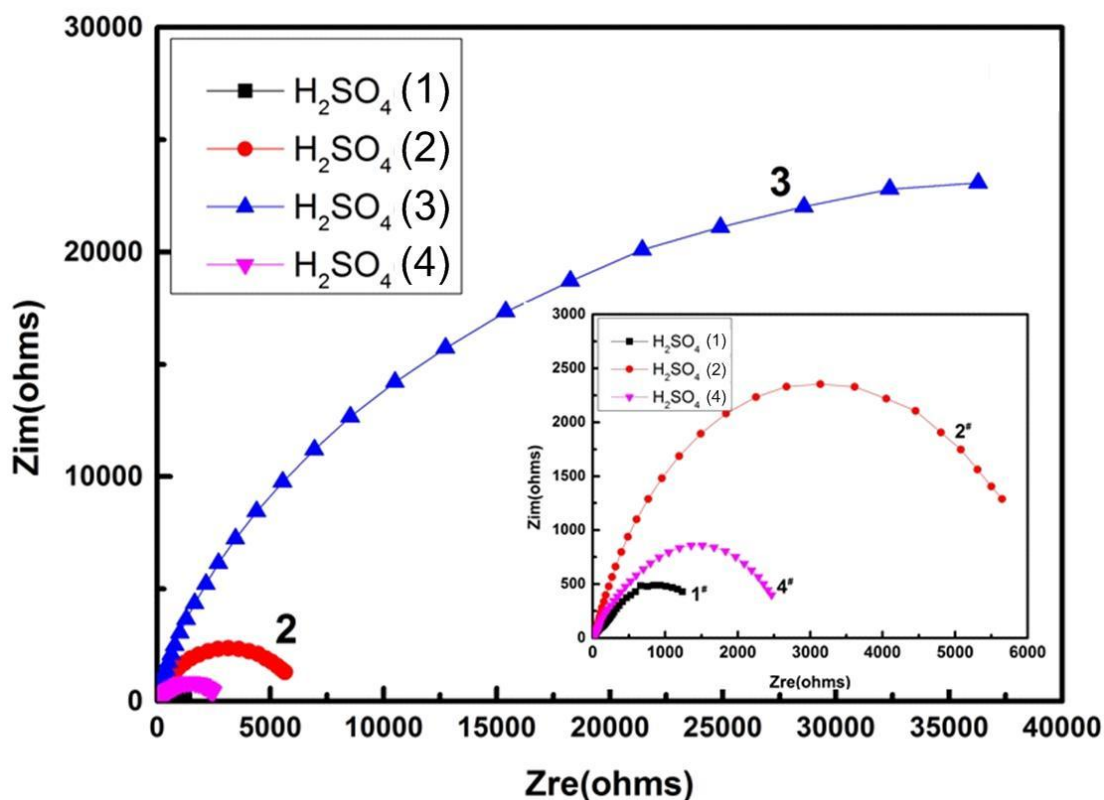


Figure 5. Electrochemical impedance spectroscopy of $\text{Co}_{68}\text{Fe}_{7-x}\text{Cr}_x\text{Si}_{15}\text{B}_{10}$ alloys in 5% H_2SO_4 solution: (1) $\text{Co}_{68}\text{Fe}_7\text{Si}_{15}\text{B}_{10}$, (2) $\text{Co}_{68}\text{Fe}_{5.5}\text{Cr}_{1.5}\text{Si}_{15}\text{B}_{10}$, (3) $\text{Co}_{68}\text{Fe}_4\text{Cr}_3\text{Si}_{15}\text{B}_{10}$ and (4) $\text{Co}_{68}\text{Fe}_{2.5}\text{Cr}_{4.5}\text{Si}_{15}\text{B}_{10}$.

3.3.4 Surface morphology after corrosion test

The surface morphologies of $\text{Co}_{68}\text{Fe}_{7-x}\text{Cr}_x\text{Si}_{15}\text{B}_{10}$ alloys after corrosion test were examined by SEM. The surface of $\text{Co}_{68}\text{Fe}_7\text{Si}_{15}\text{B}_{10}$ was found to be corroded seriously. $\text{Co}_{68}\text{Fe}_{5.5}\text{Cr}_{1.5}\text{Si}_{15}\text{B}_{10}$ presents an intensive pitting corrosion character and a large number of pitting holes can be found in the surface. Comparing with $\text{Co}_{68}\text{Fe}_{5.5}\text{Cr}_{1.5}\text{Si}_{15}\text{B}_{10}$ and $\text{Co}_{68}\text{Fe}_{2.5}\text{Cr}_{4.5}\text{Si}_{15}\text{B}_{10}$, $\text{Co}_{68}\text{Fe}_4\text{Cr}_3\text{Si}_{15}\text{B}_{10}$ shows an improved

corrosion resistance although pitting corrosion characters and localized corrosion morphology still can be found in the surface.

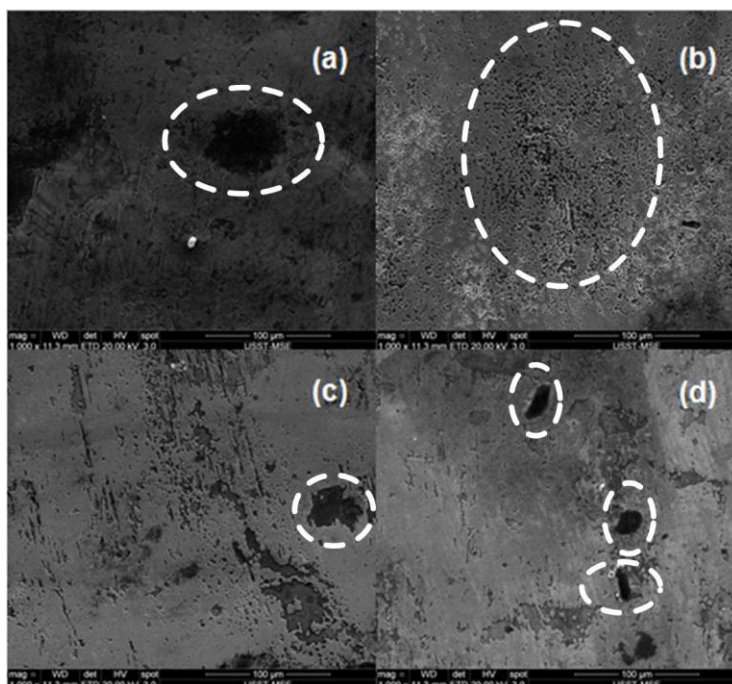


Figure 6. Surface morphologies of $\text{Co}_{68}\text{Fe}_{7-x}\text{Cr}_x\text{Si}_{15}\text{B}_{10}$ alloys after corrosion test: (a) $\text{Co}_{68}\text{Fe}_7\text{Si}_{15}\text{B}_{10}$, (b) $\text{Co}_{68}\text{Fe}_{5.5}\text{Cr}_{1.5}\text{Si}_{15}\text{B}_{10}$, (c) $\text{Co}_{68}\text{Fe}_4\text{Cr}_3\text{Si}_{15}\text{B}_{10}$ and (d) $\text{Co}_{68}\text{Fe}_{2.5}\text{Cr}_{4.5}\text{Si}_{15}\text{B}_{10}$.

4. CONCLUSION

$\text{Co}_{68}\text{Fe}_{7-x}\text{Cr}_x\text{Si}_{15}\text{B}_{10}$ ($x=0, 1.5, 3, 4.5$) amorphous ribbons were prepared by melt-spinning technique. The effect of Cr on the soft magnetic property and corrosion resistance were comprehensively investigated. The results show that Co-Fe-Cr-Si-B amorphous alloys have good glass forming ability (GFA). After adding Cr elements, the coercivity of alloys was decreased significantly. The addition of Cr element can greatly improve the corrosion resistance of Co-Fe-Si-B amorphous alloys. $\text{Co}_{68}\text{Fe}_4\text{Cr}_3\text{Si}_{15}\text{B}_{10}$ has the best soft magnetic property and lowest hysteresis loss with significant improved corrosion resistance among four different kinds of amorphous samples.

ACKNOWLEDGEMENT

The work is supported by the financial support from the National Natural Science Foundation of China (No. 51202146), the Shanghai Municipal Education Commission (No. 5114310102), the China Postdoctoral Science Foundation (No.2013M531849), the Science and Technique Foundation of ChangZhou (No.CJ20130017) and the Open Project for the Key Laboratory of Jiangsu Provincial Solar-Cell Materials and Technology (No.201202).

Reference

1. M.H. Phan, H.X. Peng, S.C. Yu and N. Chau, *Status. Solidi. A*, 201 (2004) 1558

2. M.H. Phan, Y.S. Kim, N.X. Chien, S.C. Yu, H.B. Lee and N. Chau, *Jpn. J. Appl. Phys*, 42 (2003) 5571
3. S.M. Hoque, A. Haque, M.O. Rahman, N.H. Nghi, M.A. Hakim and S. Akhter, *J. Non-Cryst. Solids*, 357 (2011) 2109
4. S. Atalay, H. Kaya, F.E. Atalay and E. Aydogmus, *J. Alloys Comp*, 561 (2013) 71
5. Z. Tang, Y. Song, S. Sun, T. Zhang and Y. Jiang, *Nanoscale*, 4 (2012) 386
6. S. Manjura Hoque, M.A. Hakim and F.A. Khan, *Phys. Status. Solidi*, 203 (2006) 336
7. Y. Song, M. Jia, M. Lin, X. Li and W. Lu, *J. Alloys. Comp*, 622 (2015) 500
8. W. Lu, Y. Xu, J. Shi, Y. Song and X. Li, *J. Alloys. Comp*, 638 (2015) 233
9. W. W. Chen and W. Gao, *Electrochim. Acta*, 55 (2010) 6865
10. R. A. Shakoor, R. Kahraman, U. Waware, Y. X. Wang and W. Gao, *Int. J. Electrochem. Sci.*, 9 (2014) 5520
11. Y.X. Wang, W.W. Chen¹, A. Shakoor, R. Kahraman, W. Lu, B. Yan and Wei Gao, *Int. J. Electrochem. Sci.*, 9 (2014) 4384
12. X. Li, W. Lu, Y. X. Wang, B. Yan, and D. Pan, *Modern Physics Letters B*, 27 (2013) 1341030
13. G.Y. Koga, R.P. Nogueira, V. Roche, A.R. Yavari, A.K.Melle, J. Gallego, C. Bolfarini, C.S. Kiminami and W.J. Botta, *Surface & Coatings Technology*, 254 (2014) 238
14. A. Baron, D. Szewieczek and G. Nawrat, *Electrochimica Acta*, 52 (2007) 5690
15. Y. J. Qin, Y. P. Wu, J. F. Zhang, W. M. Guo, S. Hong and L. Y. Chen, *Trans. Nonferrous Met. Soc. China*, 25(2015) 1144
16. Z. H. Dan, K. Takenaka, Y. Zhang, S. Unami, A. Takeuchi, N. Hara and A. Makino, *Journal of Non-Crystalline Solids*, 402 (2014) 36